Journal of
Materials Chemistry C

Accepted Manuscript

ROYAL SOCIETY OF CHEMISTRY

rsc.li/materials-c

View Article Online
DOI: 10.1039/C8TC02936A

Journal of Materials Chemistry C

ARTICLE

Triphenylamine disubstituted naphthalene diimide: elucidation of excited states involved in TADF and application in near-infrared organic light emitting diodes †

Received 00th January 20xx,
Accepted 00th January 20xx

DOI: 10.1039/x0xx00000x

www.rsc.org/

Heather F. Higginbotham,[a*] Piotr Pander,[a] Renata Rybakiewicz,[b] Marc K. Etherington,[a] Subashani Maniam,[c] Malgorzata Zagorska,[d] Adam Pron,[d] Andrew P. Monkman[a], Przemyslaw Data[a,e,f*].

It is demonstrated that naphthalene diimide core disubstituted with triphenylamine can be used as a Thermally Activated Delayed Fluorescence emitter in Organic Light Emitting Diodes. Detailed spectroscopic studies demonstrated unusual host effects on the photophysical properties of this material. In particular, we were able to deduce recombination pathways and the role of the host and temperature in increasing/decreasing the TADF contribution in overall emission. Further, stemming from these host effects on the geometry of the emitter we discover different local triplet states involved in TADF mechanism. We elucidate this confusing situation to show that simply measuring low-temperature phosphorescence does not always give the energy of the local triplet involved in TADF. The studies carried out in non-polar polymer and the OLED host were completed by the NIR OLED fabrication showing promising characteristics.

Introduction

The fabrication of stable, long-lived and efficient organic light-emitting diodes (OLEDs) is of vital importance due to their immense application opportunities, including lighting and flat panel displays.[1] It is for this reason that significant emphasis has been placed upon improving radiative decay efficiency, which is limited to 25% as a result of the recombination ratio of singlet excitons during electrical excitation.[2] Further efficiency increase requires exploitation of the 75% of triplet excitons also formed by electrical injection. In the past, this has been achieved using metalorganic phosphors,[3,4] which can promote radiative decay from spin-forbidden triplet states to obtain phosphorescent emission. However, this method requires the use of expensive and often unstable coordination compounds such as iridium and platinum complexes which induce spin-orbit coupling (SOC).

Recently, thermally-activated delayed fluorescence (TADF), or E-type delayed fluorescence, has been identified as an alternative method for harvesting triplet excitons, through the use of fast reverse intersystem crossing (rISC) between energetically close triplet and singlet states.[5,6,7] This mechanism can give rise to near 100% internal quantum efficiency[2,6] using purely organic luminophores, opening the doorway for cheap OLED fabrication. Furthermore, TADF emitting OLEDs have also been synthesised in a variety of colour outputs, required for the fabrication of soft white lighting, despite difficulties to obtain blue[8-10] and red[11] emitting diodes.

Materials extensively used as red-emitting dyes are the core-substituted 1,4,5,8-tetracarboxylic naphthalene diimides (cNDIs), as a substitution in the 2 and 6 or 2, 3, 6, and 7 positions of the core with electron donating groups can render a red/near IR emissive output.[12-14] As well as their use as red emitting sensing[15-17] and single molecule[18,19] materials, cNDIs and other arylene diimides have been extensively used in electroactive applications[20] such as organic field-effect transistors (OFETs). Arylene diimides core-substituted with electron attracting groups are suitable for the fabrication of air-stable *n*-channel OFETs[21] whereas those containing electron donating groups yield ambipolar transistors.[22] These materials can also be used in solar cells,[23-26] as their rigid, electron deficient poly-aromatic hydrocarbon core provide suitable electron-mobility and thermal stability. This allows them to easily form predominantly *n*-type semiconductors. Many of these photovoltaic devices have been shown to meet the requirements of practical industrial applications including long-term air-stability, and predictable redox and solid state properties. Furthermore, functionalisation of cNDIs allows for the formation of a plethora of derivatives that can be optimized to fit desired photophysical and electrochemical outputs. Although to this point never used in OLED applications, NDIs have found a home in many donor-acceptor based systems, (most especially in porphyrin-NDI

[a] Physics Department, Durham University, South Road, Durham, DH1 3LE, United Kingdom. *E-mail: Przemyslaw.Data@dur.ac.uk
[b] Cardinal Stefan Wyszynski University in Warsaw, Faculty of Mathematics and Natural Sciences. School of Exact Sciences, Wóycickiego 1/3 building 21, 01-938 Warsaw, Poland
[c] School of Chemistry, Monash University, Clayton, Victoria, Australia
[d] Faculty of Chemistry Warsaw University of Technology, Noakowskiego 3, 00-664 Warsaw, Poland
[e] Faculty of Chemistry, Silesian University of Technology, Ks. M. Strzody 9, 44-100 Gliwice, Poland. *E-mail: Przemyslaw.Data@polsl.pl
[f] Centre of Polymer and Carbon Materials, Polish Academy of Sciences, M. Curie-Sklodowskiej 34, 41-819 Zabrze, Poland

† Electronic Supplementary Information (ESI) available: experimental details, additional photophysics results. See DOI: 10.1039/x0xx00000x

based dyads).[27-29] In these dyads, they form photoinduced intramolecular charge-separated states - a molecular requirement for the fabrication of many TADF OLED materials.

The design of TADF materials that cater towards specific OLED device manufacture requires the critical arrangement of the local triplet (^{3}LE) and charge-transfer states (^{1}CT and ^{3}CT) to promote the spin-vibronic coupling that underpins rISC and TADF.[30-32] This mechanism involves vibronic coupling between the ^{3}LE and ^{3}CT that then mediates the rISC mechanism in the CT manifold. It has become common knowledge that the arrangement and reduction, creating a small $\Delta E_{S\text{-}T}$ gap, is crucial to the efficiency of this process. However, even when so much is understood on the energetics of the emissive and host materials, promising photophysical results are often met with poor electroluminescence output. This is often due to the host and emissive material being considered separately, however, the effect of the host on the energetics of the emissive states should not be overlooked.[10]

Here we present a set of photophysical measurements to resolve an initially observed disconnect between strong TADF output seen in a newly synthesised red 'TADF' emitter, **TPA-cNDI** (**Figure 1**), in a host that forms a moderately large $\Delta E_{S\text{-}T}$ and the poor emission output in a host that forms an assumed smaller $\Delta E_{S\text{-}T}$. Using both temperature dependent emission and quasi-CW photoinduced absorption, different local triplet states (^{3}LE) are identified. Using data measured from the donor and acceptor subunits in combination with the emitter, however, allowed us to correctly identify the coupling triplet states to yield a more accurate measure of $\Delta E_{S\text{-}T}$ related to the DF process. Using this knowledge, a more strategic synthetic approach for efficient TADF based OLED devices may be developed in the future.

Experimental Methods

The synthesis procedure for **TPA-cNDI** is given in the literature.[33] The solvents, methylcyclohexane (MCH) and toluene were purchased from Romil whereas tetrahydrofuran (THF) was purchased from Sigma Aldrich (analytical grade). They were used without further purification.

Steady-state photophysical measurements were performed in dilute solutions, with UV-visible absorption spectra taken upon a UV-3600 Shimadzu spectrophotometer and emission spectra taken upon a Jobin Yvon Horiba Fluoromax-3. The emission spectra were calibrated for detector efficiency using instrument specific company calibration files. Photoluminescence quantum yield of **TPA-cNDI** was recorded in MCH using a method described in previous works.[34,35] Fluorescein in 0.1 M NaOH was used as a standard (φ = 0.90).[36,37]

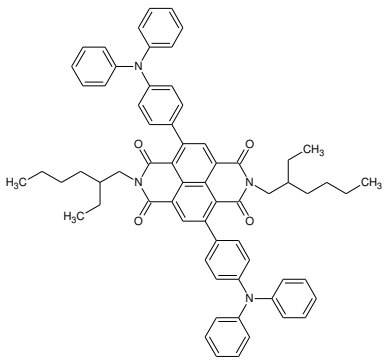

Figure 1 Investigated molecule, **TPA-cNDI.**

Time-resolved photophysical measurements are described elsewhere.[38] The excitation source for all temperature dependent/ time-resolved measurements was the 3rd harmonic of a Nd:YAG laser (355 nm) (EKSPLA-SL312), while a nitrogen laser (337 nm) (LTB-MNL 100, Lasertechnik Berlin) was used for power dependent measurements due to its superior stability. Solid-state samples used in this analysis were prepared as a 1% w/w ratio in zeonex or a 10% w/w ratio in CBP, dropcast from toluene onto clean quartz substrates at 90 °C on a hotplate until dry.

For the measurement of the quasi-continuous photo-induced absorption, 375 nm laser excitation light (Vortran Stradus 375-60), modulated at 73 Hz supplied by a lock-in amplifier (Signal Recovery 7225), was passed through the sample, acting as the pump source. Simultaneously, a continuous wave laser-driven white light source (ENERGETIQ EQ-99CAL), was used as a probe. The probe beam after passing through the sample passed through a monochromator (Bentham TMc300) and collected on a silicon detector connected to the lock-in amplifier, both ac and dc probe signals are measured by the lock-in. Using this apparatus, the spectral change in absorption with and without the pump was obtained, allowing measurement of transitions from excited states to higher excited states in the studied system. $\Delta T/T$ output as a function of wavelength was then calculated using an in-house lab-view program.[31]

Samples suitable for quasi-CW analysis were prepared by drop-casting the blend of **TPA-cNDI** and the host onto a quartz substrate. For the zeonex sample, a blend of 0.27 mg/mL solution of **TPA-cNDI** and 127 mg/ml solution of zeonex was mixed 1:1, producing a 0.21% w/w film. For the OLED host sample, **TPA-cNDI** and the host were mixed in a 1:9 ratio by weight in toluene and drop cast onto quartz substrates.

Results and discussion

Figure 2 shows normalized steady-state UV-visible and emission spectra of **TPA-cNDI** in MCH, toluene and THF. The absorption spectra in all solvents show a high energy, strongly vibronic band (onset at 399 nm in MCH) common to arylene diimides which do not contain core substituents.[12,13,39] Concurrently, a low energy band is observed in all solvents with a peak maxima shift and an onset absorbance of 659 nm (1.88 eV), 685 nm (1.81 eV), and 685 nm (1.81 eV) in MCH, toluene and THF respectively. This low energy band has been observed in a large range of core-substituted NDIs but is not present in non-substituted NDIs. Common substituents which induce this new absorption band include electron donating groups such as aliphatic and aromatic amines which can be attached to the core *via* amine nitrogen[13] or *via* a phenylene linker[40] as in **TPA-cNDI,** but also phenyl or pyridine substituents.[41,42] In non-polar solvents this absorption has vibronic structure and thus as a

View Article Online
DOI: 10.1039/C8TC02076A

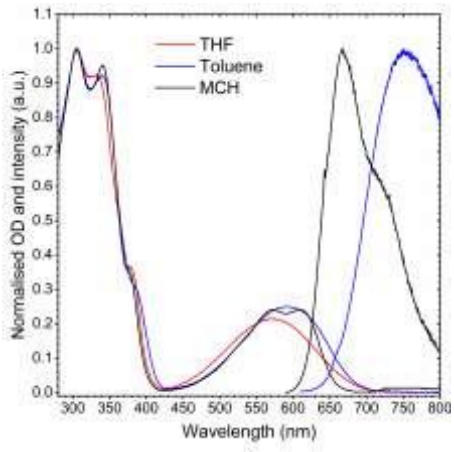

Figure 2 Normalised absorbance and emission spectra (λ_{ex}= 300 nm) of **TPA-cNDI** in MCH (black), toluene (blue) and THF (red). Note: emission spectrum of **TPA-cNDI** in THF is not observed. The concentration of all solutions was 10^{-5} M.

result of conjugation to the NDI core, absorption is through a transition from ground state to ^{1}LE. In polar solvents, the absorption loses its vibronic structure, indicative of CT character.

Due to the nature of **TPA-cNDI**, the linking phenylene ring can rotate and thus at certain times the molecule is planar and conjugated and at others, the linking ring is perpendicular to the core plane, where it promotes more traditional charge-transfer between the TPA and cNDI. The positive solvatochromic shift of the onset of this band in polar solvents indicates strong π-π* character, indicative of the nitrogen lone pair in TPA unit being delocalised over the π-conjugated system.

Steady-state emission spectra of **TPA-cNDI** show red/near-IR emission in non-polar MCH and toluene, which is not visible in highly polar solvents **(Figure 2**). Emission in MCH also has a blue component arising from the NDI core, having vibronic structure indicative of the conjugated local exciton (^{1}LE). This characteristic dual emission (see **Figure S3**) is most commonly seen in Twisted Intramolecular Charge Transfer (TICT) systems[43] but **in TPA-cNDi** we believe this is the first observation of both dual fluorescence and very strong TADF. This we attribute to weak stabilisation of the CT state in MCH and a need for some excess energy to help drive the molecule to a fully orthogonal, decoupled D-A-D structure in non-polar environments such as MCH. The enhanced LE character of the NIR CT excitation accounts for it's observed emission pseudo vibronic structure but will give a higher radiative decay rate which may explain the very strong DF component we observe. Solvatochromism of this molecule can be demonstrated by comparing its spectra recorded in MCH and toluene. In the latter case, the emission band displays a Gaussian profile and is red shifted, which can be identified as emission from a CT state. This is further supported by the geometry-optimised structure of **TPA-cNDI**, computationally determined to exhibit close to 90-degree torsion angle between the NDI core and the phenylene ring linking the triphenylamine substituent with this core, which enhances CT state formation.[22]

Inspection of time-resolved/temperature dependent spectroscopy in a solid zeonex matrix (containing 1% w/w of **TPA-cNDI**), shows that the prompt emission decays with a lifetime of 1.9 ns, indicative of fast singlet excited state decay (**Figure 3b**). The prompt lifetime increases to 3.0 ns on cooling to 80 K. This indicates the strong effect that non-radiative relaxation plays on photoluminescence of **TPA-cNDI** and thus explains the low photoluminescence quantum yield at 300 K, Φ_{PL} = 8.4% (in MCH). The spectra relating to this fast component have an onset energy of 1.97 eV. At 300 K, the strong delayed emission is observed, with delayed fluorescence to prompt fluorescence (DF/PF) ratio of 9.6 and an identical spectrum to the prompt component in both shape and emission onset (see **Figure 3a**). This delayed decay can be fit to two lifetimes of 3.1 and 25.9 μs (**Figure 3b**) and is identified as TADF through the spectral analysis of the delayed emission and laser power dependence of the emission (**Figure S1d**).

By cooling the same film of **TPA-cNDI** in zeonex down to 80 K, one can observe a long-delayed component with a lifetime of 379 μs, and an onset energy of 1.79 eV (see **Figure 3a and b**). This near IR-emitting species is significantly temperature and oxygen sensitive and is spectrally determined to be distinct from the TADF emission, thus is identified as phosphorescence. Using the energy onset as an indicator, we find that this emissive triplet state species has neither unique triplet character of the donor TPA moiety (^3LE_D) nor the NDI acceptor one (^3LE_A), as is often observed in exclusively electronic decoupled donor and acceptor TADF materials.[44] This means that within some conformations of the molecules there is significant orbital mixing between the donor and the acceptor units, forming a new molecular species.[45] Using the energy difference between the observed ^{1}CT state and a $^3LE_{Con}$ (a triplet state from the more conjugated planar molecular species) phosphorescence, the ΔE_{S-T} of **TPA-cNDI** in zeonex is found to be 180 meV, resulting in a rISC process that creates the observed delayed emission. The energy of the $^3LE_{Con}$ state will rise upon decrease of the conjugation to become identical with ^3LE_A when the D and A species are perfectly orthogonal (note this refers to excited, not ground state geometry). Although the $^3LE_{Con}$ cannot fully be attributed as a local triplet state, its resemblance to the classical local states is still significant, thus we use the term "local" and "LE" also to describe this type of excited state.

In the spectrum of a CBP film containing 10% of **TPA-cNDI,** a bathochromic shift of the CT band is observed, which should in principle push the ^{1}CT state closer in energy to this lowest energy triplet state, bringing with it an enhancement of TADF. However, this is not what is observed, as delayed emission output of **TPA-cNDI** in CBP is dramatically reduced (**Figure 3d** and **Figure S2**) even though the onset energy of the prompt and delayed emission is bathochromically shifted to 1.87 eV at room temperature and the onset of the observed phosphorescence at 80 K remains almost unchanged (1.77 eV) (**Figure 3c**). This creates an assumed ΔE_{S-T} of 100 meV between the ^{1}CT state and the $^3LE_{Con}$ state. Using the time-resolved analysis of **TPA-cNDI** in CBP, prompt and delayed fluorescence lifetimes were estimated to be 1.2 ns and 10 μs at 300 K respectively. The DF/PF ratio of **TPA-cNDI** in this film is estimated to be only 6.2, which is lower than that observed in zeonex, highlighting a less

efficient rISC process. The phosphorescence emission in the CBP film at 80 K was too weak to estimate its lifetime. Two further observations can be seen from this CBP data. First, the spectra are far noisier than in zeonex showing a much reduced PLQY, and also at 80 K, the spectra are very different. The prompt emission, as seen in **Figure 3c**, is clearly a narrow Gaussian band that is highly redshifted, onset at 1.8 eV. No higher energy emission, as observed at RT is observed. This we ascribed to hindered ring torsion motion at low temperature in the more rigid and dense CBP film. Since this low-temperature band is red-shifted with respect to the high-temperature emission we ascribed it to the more conjugated molecular species, implying that thermal energy is required to disrupt the NDI planarity in a rigid matrix.

Lower DF/PF ratio in CBP could be ascribed to more intensive non-radiative decay caused by aggregation and π-π stacking of the molecules. A slight decrease of triplet energy by 0.02 eV could also decrease its lifetime (vide energy gap law).

To further understand the discrepancy between the experimental data and current theory (that smaller ΔE_{S-T} results in a faster rISC rate) we first look at the molecular structure of **TPA-cNDI**. The HOMO and LUMO of **TPA-cNDI** are discreet, electronically decoupled orbitals, with the LUMO residing on the core of the NDI and the HOMO located on the triphenylamine moieties, supporting CT formation.[22] This electronic configuration not only promotes the formation of a CT state (through minimizing the molecular exchange energy) but also breaks conjugation between the donor and acceptor subunits resulting in singlet and triplet states with unique subunit character.

With this in mind, the triplet energy of the NDI and TPA subunits were found to build up a more comprehensive picture of the excited state dynamics of this molecule. The triplet energy onset of the TPA subunit (^3LE_D) was found in the literature to be 3.14 eV[46] and considered too high in energy to participate in coupling to the observed lower energy singlet state. The NDI acceptor phosphorescence (^3LE_A) was measured, onset energy

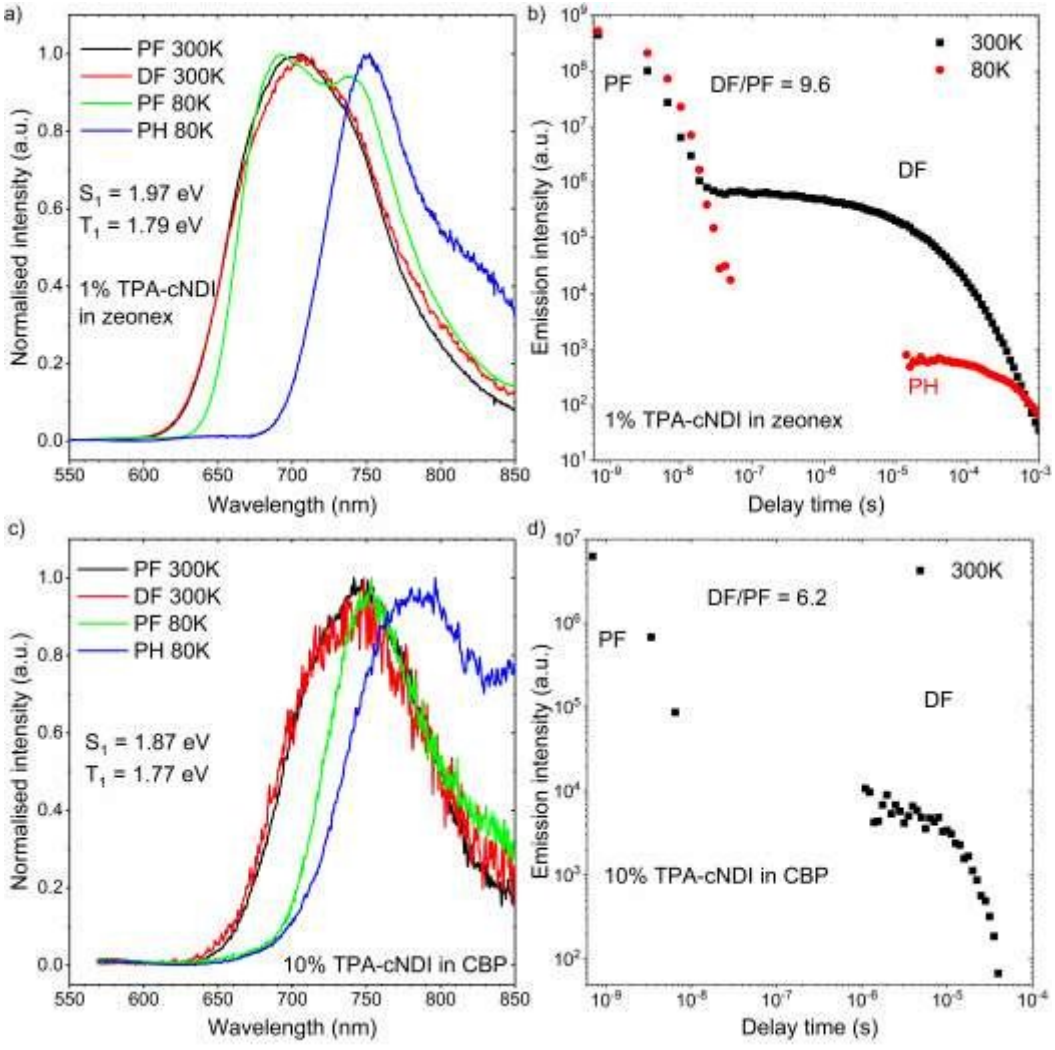

Figure 3 a) Normalised time-dependent emission spectra of 1% **TPA-cNDI** in zeonex, prompt CT fluorescence (PF) (black at 300 K), prompt CT fluorescence(green at 80 K) recorded at nanosecond delay times, delayed CT fluorescence (DF) at 300 K (red) recorded at 50 µs delay, $^3LE_{Con}$ phosphorescence (PH) at 80 K (blue) recorded at 1 ms delay. b) Graph of emission intensity against time at 300 K (black) and 80 K (red) of 1% TPA-**cNDI** in zeonex, gap in nanosecond-microsecond region is related to low signal to noise ratio at particular delay time. c) Normalised time-dependant emission spectra of 10% TPA-**cNDI** in CBP, prompt CT fluorescence (PF) (black at 300 K, prompt CT fluorescence (green at 80 K) recorded at nanosecond delay times, delayed CT fluorescence (DF) at 300 K (red) recorded at 3 µs delay, $^3LE_{Con}$ phosphorescence (PH) at 80 K (blue) recorded at 10 µs delay with 10 ms integration time. d) Graph of emission intensity against time at 300 K (black) of 10% **TPA-cNDI** in CBP, gap in nanosecond-microsecond region is related to low signal to noise ratio at particular delay time .

View Article Online
DOI: 10.1039/C8TC02936A

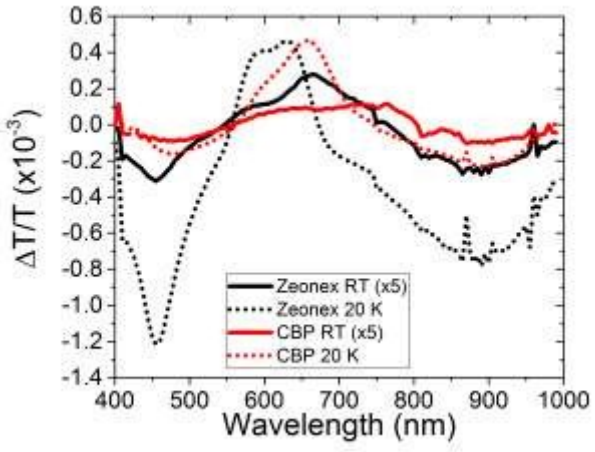

Figure 4 The in-phase component of the PIA for **TPA-cNDI** in zeonex and CBP. The room temperature signal is very weak and has been amplified by a factor of five for both hosts. However, it can be seen that the PIA appears in a similar position to the 20 K measurements. There are clearly two strong absorption bands, one well defined peak near 460 nm and a broader absorption around 880 nm.

of 2.13 eV (**Figure S4**) with a strong vibronic structure to the phosphorescence. As stated above both of these triplet emissions are very different from the observed **TPA-cNDI** triplet spectrum. The ^3LE_A state as sufficiently close to the CT can participate in rISC as a mediator state, thus reducing the effective energy gap.[47]

This argument is further validated through an inspection of an Arrhenius plot, with experimental points measured from 280 K to 80 K at 1 µs delay time. This plot, obtained for the same zeonex film, reveals an activation energy of 0.082 eV (**Figure S1c**), which is closer to the energy gap between ^{1}CT and ^3LE_A, thus providing evidence that the pure acceptor triplet state could be the mediator for TADF. At this point, it has to be said that the rISC can either be mediated via the ^3LE_A state or proceed without a mediator, however slower, directly from the $^3LE_{Con}$.

To prove the presence of NDI local triplet (^3LE_A or $^3LE_{Con}$) in **TPA-cNDI** we turn to the information-rich quasi-CW photoinduced absorption technique. The spectra for **TPA-cNDI** in both zeonex and CBP at room temperature and 20 K are shown in **Figure 4**. First, it is apparent that, for both hosts, the signal is much weaker at room temperature than low temperature (the room temperature signal is multiplied by a factor of five in **Figure 4**). In both zeonex and CBP samples, two PIA peaks can be distinguished, located at approximately 460 nm and 880 nm. The well-defined peak at 460 nm has been assigned to the T_1-T_N transition of the local exciton triplet absorption on the NDI acceptor which can either reflect $^3LE_{Con}$ or ^3LE_A triplet population. The broader peak at 880 nm can be ascribed to the absorption within the charge-transfer states of this system. Similar lower energy broad absorption bands were found in TADF molecules showing a strong presence of CT states.[31,48]

The positive signal observed in both hosts is the ground state bleaching (GSB) of the absorption in these systems. It is immediately obvious that the PIA spectrum is similar to the ground state absorption of **TPA-cNDI** in zeonex and CBP. For zeonex especially, the GSB is similar to the absorption in MCH, confirming similar polarity of the host and the solvent. The small

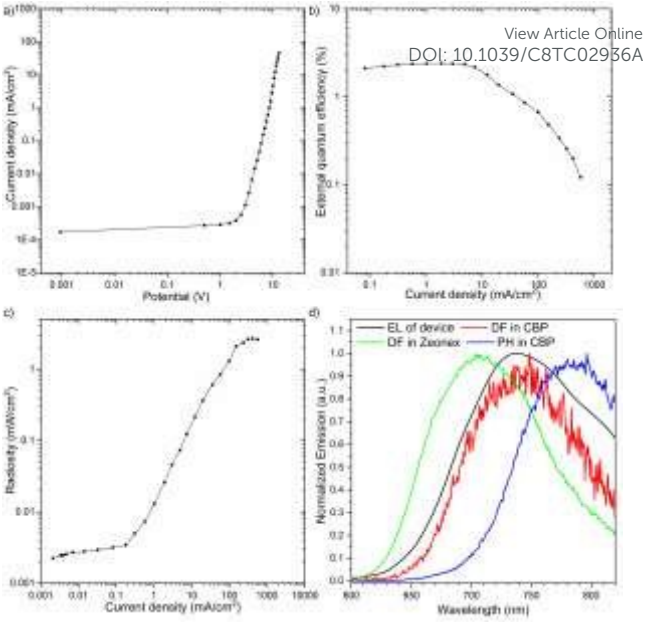

Figure 5 a-c) Characteristics of OLED devices fabricated using emitters and host presented in this work, d) comparison of electroluminescence and photoluminescence spectra.

red-shift measured in the CBP host as compared to the zeonex one is consistent with the red shift in the ^{1}CT emission at 80 K for these materials (See **Figure 3a and c**). Host comparison shows that there is a much stronger triplet absorption at 460 nm and also more intense CT absorption above 750 nm in the zeonex host. This is attributed to the ^3LE_A and CT states being closer together in the zeonex host as emphasised by the cNDI triplet energy of 2.13 eV and highlights the issue in using the observed phosphorescence in the ΔE_{S-T} calculation without careful consideration.

In the fabrication of OLED devices (**Figure 5**) the following configuration of layers was used with the goal to optimize the hole to electron ratio: ITO/NPB(40 nm)/TAPC (10 nm)/10% **TPA-cNDI** co CBP (20 nm)/TPBi(10 nm)/PO-T2T(40 nm)/LiF(1 nm)/Al(100 nm). The diode characteristics are presented in **Figure 5.** As for the NIR region of the OLED emission, the radiosity instead of luminance was chosen to evaluate the emission. The devices show radiosity turn-on voltage at 5 V and current turn-on 3.0 V. The device emitting in the high NIR band exhibited EQE of 2.4 % and radiosity of 2.7 mW/cm^2 due to triplet harvesting by the TADF mechanism.

Conclusions

To summarize, in the search for new near-infrared emitting TADF electroluminophores we have investigated the excited states and relaxation processes of a triphenylamine naphthalene diimide in solutions and in solid hosts of different polarity. In particular, the presented results underline the importance of elucidating all unique excited state energies within a molecular system in order to accurately comprehend the depopulation mechanisms within a single emitting species.

In **TPA-cNDI** it is clear that molecular geometry is crucial. There is a state existing due to a more planar, conjugated geometry having a high degree of excitonic delocalisation in contrary to

more define uncoupled donor and acceptor units. In the planar configuration, the lowest energy triplet state of the molecule is a unique molecular state of low energy, $^3LE_{Con}$, onset at 1.79 eV, different from the normal local triplet of the NDI core. Nevertheless, given that we understand these issues, it was possible to demonstrate efficient NIR emitting TADF based OLED devices with good efficiency for the infra-red region using **TPA-cNDI**.

Conflicts of interest

There are no conflicts to declare

Acknowledgements

P.P. thanks to the European Union for financial support from H2020-MSCA-ITN-2015 / 674990 EXCILIGHT grant. A.P. and M.Z. wish to acknowledge financial support from National Science Centre, Poland, (NCN) Grant No. 2015/17/B/ST5/00179. P.D. acknowledges the EU's Horizon 2020 for funding the ORZEL project under grant agreement No 691684. H.H and M.K.E acknowledge the EU's Horizon 2020 for funding the PHEBE project under grant agreement No. 641725.

Notes and references

1 Y. Tao, K. Yuan, T. Chen, P. Xu, H. Li, R. Chen, C. Zheng, L. Zhang and W. Huang, *Adv. Mater.* 2014, **26**, 7931-7958.
2 F. B. Dias, K. N. Bourdakos, V. Jankus, K. C. Moss, K. T. Kamtekar, V. Bhalla, J. Santos, M. R. Bryce and A. P. Monkman, *Adv. Mater.*, 2013, **25**, 3707–3714.
3 M. A. Baldo, D. F. O'Brien, Y. You, A. Shoustikov, S. Sibley, M. E. Thompson and S. R. Forrest, *Nature*, 1998, **395**, 151–154.
4 M. A. Baldo, M. E. Thompson and S. R. Forrest, *Nature* 2000, **403**, 750-753.
5 M. N. Berberan-Santos and J. M. M. Garcia, *J. Am. Chem. Soc.*, 1996, **118**, 9391–9394.
6 H. Uoyama, K. Goushi, K. Shizu, H. Nomura and C. Adachi, *Nature*, 2012, **492**, 234–238.
7 G. Méhes, H. Nomura, Q. Zhang, T. Nakagawa and C. Adachi, *Angew. Chem. Int. Ed.* 2012, **51**, 11311-11315.
8 Q. Zhang, B. Li, S. Huang, H. Nomura, H. Tanaka and C. Adachi, *Nat. Photon.* 2014, **8**, 326-332.
9 M. Kim, S. K. Jeon, S. H. Hwang, J. Y. Lee, *Adv. Mater.* 2016, **28**, 603-603.
10 P. L. dos Santos, J. S. Ward, M. R. Bryce and A. P. Monkman, *J. Phys. Chem. Lett.*, 2016, **7**, 3341–3346.
11 S. Hirata, Y. Sakai, K. Masui, H. Tanaka, S. Y. Lee, H. Nomura, N. Nakamura, M. Yasumatsu, H. Nakanotani, Q. Zhang, K. Shizu, H. Miyazaki and C. Adachi, *Nat. Mater.* 2015, **14**, 330-336.
12 F. Würthner, S. Ahmed, C. Thalacker and T. Debaerdemaeker, *Chem. Eur. J.* 2002, **8**, 4742-4750.
13 N. Sakai, J. Mareda, E. Vauthey and S. Matile, *Chem. Commun.* 2010, **46**, 4225-4237.
14 C. Thalacker, C. Roger and F. Würthner, *J. Org. Chem.* 2006, **71**, 8098-8105.
15 X. Lu, W. Zhu, Y. Xie, X. Li, Y. Gao, F. Li and H. Tian, *Chem. Eur. J.* 2010, **16**, 8355-8364.
16 R. P. Cox, H. F. Higginbotham, B. A. Graystone, S. Sandanayake, S. J. Langford and T. D. M. Bell, *Chem. Phys. Lett.* 2012, **521**, 59-63.
17 S. Maniam, H. F. Higginbotham, S. X. Guo, T. D. M. Bell, E. I. Izgorodina and S. J. Langford, *Asian J. Org. Chem.* 2014, **3**, 619-623.
18 T. D. M. Bell, S. Yap, C. H. Jani, S. V. Bhosale, J. Hofkens, F. C. De Schryver, S. J. Langford and K. P. Ghiggino, *Chem. Asian J.* 2009, **4**, 1542-1550.
19 S. Maniam, R. P. Cox, S. J. Langford and T. D. M. Bell, *Chem. Eur. J.* 2015, **21**, 4133-4140.
20 S. Maniam, H. F. Higginbotham, T. D. M. Bell and S. J. Langford, *Naphthalenediimide and its Congeners: From Molecules to Materials*; The Royal Society of Chemistry, 2017; pp 244-276.
21 F. Würthner and M. Stolte, *Chem. Commun.* 2011, **47**, 5109-5115.
22 A. Pron, R. R. Reghu, R. Rybakiewicz, H. Cybulski, D. Djurado, J. V. Grazulevicius, M. Zagorska, I. Kulszewicz-Bajer and J. M. Verilhac, *J. Phys. Chem. C* 2011, **115**, 15008-15017.
23 L. Le Pleux, A. L. Smeigh, E. Gibson, Y. Pellegrin, E. Blart, G. Boschloo, A. Hagfeldt, L. Hammarstrom and F. Odobel, *Energy Environ. Sci.* 2011, **4**, 2075-2084.
24 E. Ahmed, G. Ren, F. S. Kim, E. C. Hollenbeck and S. A. Jenekhe, *Chem. Mater.* 2011, **23**, 4563-4577.
25 M. Yuan, M. M. Durban, P. D. Kazarinoff, D. F. Zeigler, A. H. Rice, Y. Segawa and C. K. Luscombe, *J. Polym. Sci. Part A: Polym. Chem.* 2013, **51**, 4061-4069.
26 T. Earmme, Y. J. Hwang, N. M. Murari, S. Subramaniyan and S. A. Jenekhe, *J. Am. Chem. Soc.* 2013, **135**, 14960-14963.
27 S. J. Langford, M. J. Latter and C. P. Woodward, *Photochem. Photobiol.* 2006, **82**, 1530-1540.
28 B. Robotham, K. A. Lastman, S. J. Langford and K. P. Ghiggino, *J. Photoch. Photobiol. A* 2013, **251**, 167-174.
29 O. Yushchenko, R. V. Hangarge, S. Mosquera-Vazquez, S. Boshale and E. Vauthey, *J. Phys. Chem. B* 2015, **119**, 7308-7320.
30 J. Gibson, A. P. Monkman and T. J. Penfold, *ChemPhysChem* 2016, **17**.
31 M. K. Etherington, J. Gibson, H. F. Higginbotham, T. J. Penfold and A. P. Monkman, *Nat. Commun.*, 2016, **7**, 13680.
32 E. Angioni, M. Chapran, K. Ivaniuk, N. Kostiv, V. Cherpak, P. Stakhira, A. Lazauskas, S. Tamulecius, D. Volyniuk, N.J. Findlay, T. Tuttle, J.V. Grazulevicius and P.J. Skabara. *J. Mater. Chem. C* 2016, **4**, 3851-3856.
33 R. Rybakiewicz, P. Gawrys, D. Tsikritzis, K. Emmanouil, S. Kennou, M. Zagorska and A. Pron, *Electrochim. Acta*, 2013, **96**, 13–17.
34 A. T. R. Williams, S. A. Winfield and J. N. Miller, *Analyst* 1983, **108**, 1067-1071.
35 P. Data, A. Kurowska, S. Pluczyk, P. Zassowski, P. Pander, R. Jedrysiak, M. Czwartosz, L. Otulakowski, J. Suwinski, M. Lapkowski and A. P. Monkman, *J. Phys. Chem. C* 2016, **120**, 2070-2078.
36 G. A. Crosby and J. N. Demas, *J. Phys. Chem.* 1971, **75**, 991-1024.
37 L. Porrès, A. Holland, L. O. Pålsson, A. P. Monkman, C. Kemp and A. Beeby, *J. Fluoresc.* 2006, **16**, 267-273.
38 C. Rothe and A. P. Monkman, *Phys. Rev. B* 2003, **68**, 075208.
39 S. V. Bhosale, C. H. Jani and S. J. Langford, *Chem. Soc. Rev.* 2008, **37**, 331-342.
40 S. Pluczyk, P. Zassowski, R. Rybakiewicz, R.Wielgosz, M. Zagorska, M. Lapkowski and A. Pron, *RSC Advances* 2015, **5**, 7401-7412.
41 S. L. Suraru and F. Würthner, *Synthesis* 2009, **2009**, 1841-1845.
42 S. V. Bhosale, M. B. Kalyankar, S. V. Bhosale, S. J. Langford, E. F. Reid and C. F. Hogan, *New J. Chem.* 2009, **33**, 2409-2413.
43 S. Sasaki, G. P. C. Drummen and G.-i. Konishi, *J. Mater. Chem. C* 2016, **4**, 2731-2743.

View Article Online
DOI: 10.1039/C8TC02936A

44 P. L. Santos, J. S. Ward, P. Data, A. S. Batsanov, M. R. Bryce, F. B. Dias and A. P. Monkman, *J. Mater. Chem. C* 2016, **17**, 3815-3824.
45 R. Pashazadeh, P. Pander, A. Lazauskas, F. B. Dias and J. V. Grazulevicius, *J. Phys. Chem. Lett.* 2018, **9**, 1172-1177.
46 R. D. Burkhart and N.-I. Jhon, *J. Phys. Chem.* 1991, **95**, 7189-7196.
47 J. Gibson and T. J. Penfold, *Phys. Chem. Chem. Phys.* 2017, **19**, 8428–8434.
48 T. Hosokai, H. Matsuzaki, H. Nakanotani, K. Tokumaru, T. Tsutsui, A. Furube, K. Nasu, H. Nomura, M. Yahiro, C. Adachi, *Sci. Adv.* 2017, **3**, e1603282.

View Article Online
DOI: 10.1039/C8TC02936A

Journal of Materials Chemistry C

Triphenylamine disubstituted naphthalene diimide: elucidation of excited states involved in TADF and application in near-infrared organic light emitting diodes

Heather F. Higginbotham,* Piotr Pander, Renata Rybakiewicz, Marc K. Etherington, Subashani Maniam, Malgorzata Zagorska, Adam Pron, Andrew P. Monkman, Przemyslaw Data.*

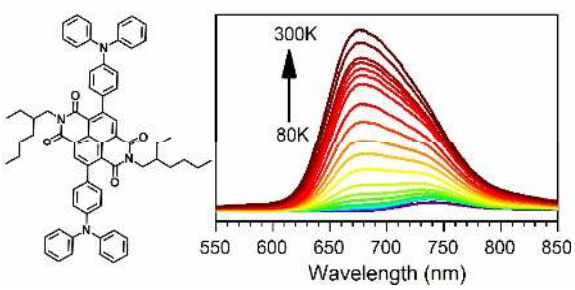

New TADF emitter is presented showing near-infrared efficient emission.